Harmonic and power balance tools for tapping-mode atomic force microscope

A. Sebastian, M. V. Salapaka,[a] and D. J. Chen
Department of Electrical and Computer Engineering, Iowa State University, Ames, Iowa 50011

J. P. Cleveland
Asylum Research, Santa Barbara, California 93117

(Received 24 August 2000; accepted for publication 19 February 2001)

The atomic force microscope (AFM) is a powerful tool for investigating surfaces at atomic scales. Harmonic balance and power balance techniques are introduced to analyze the tapping-mode dynamics of the atomic force microscope. The harmonic balance perspective explains observations hitherto unexplained in the AFM literature. A nonconservative model for the cantilever–sample interaction is developed. The energy dissipation in the sample is studied and the resulting power balance equations combined with the harmonic balance equations are used to estimate the model parameters. Experimental results confirm that the harmonic and power balance tools can be used effectively to predict the behavior of the tapping cantilever. © *2001 American Institute of Physics.* [DOI: 10.1063/1.1365440]

I. INTRODUCTION

Although dynamic modes have been known and used since the beginning of the field of atomic force microscopy,[1] it is only within the last few years that a better understanding has developed of the complicated dynamics occurring in these modes. For several years, a linear approximation was used to explain the physics of noncontact imaging. In this approximation, the cantilever amplitude was assumed to be small enough so that the tip–sample gradient could be viewed as altering the spring constant of the cantilever (all higher derivatives ignored). Although this model explains some of the basic physics associated with dynamic modes, except for long-ranged forces (for example, electric and magnetic) the approximation fails because the tip–sample potential changes appreciably over angströms as the tip and sample get very close or come into contact.

With the introduction of tapping-mode atomic force microscope (AFM),[2] the oscillating cantilever tip comes into intermittent contact with the sample and a simple linear model does not suffice. A couple of years later, the resolution of single defects using noncontact AFM in ultrahigh vacuum spurred significant development in that field. In this mode, the cantilever oscillation is at least several angströms and the tip comes within Angstroms of the sample surface. Thus again a simple linear model does not explain the dynamics. The rash of activity in both of these AFM fields prompted considerable theoretical work to explain the nonlinear dynamics.

Initially, much of the research on tapping-mode AFM centered around numerically solving nonlinear differential equations that include terms to account for the tip–sample interaction (see, for example, Ref. 3). These models were successful in capturing many of the intricate details present in most experimental data.[3] However due to their complexity, the numerical models preclude identification of model parameters in a straightforward manner. Indeed, the set of existing tools to identify a given model of the interaction from experimental data is inadequate. Another void in this area is a systematic methodology for the purposes of identification (some recent studies in this direction are pursued in Ref. 4). Of particular interest is a set of common tools that can be applied over a wide range of tapping-mode AFM applications. Such tools are particularly relevant because of the diverse variety of materials and properties that the tapping-mode AFM is used for imaging.

A surprising property of the tapping-mode dynamics is the near sinusoidal nature of the steady-state cantilever–tip oscillations. Like experimental data, this feature is predicted by the complex numerical models of the nonlinear tip–sample interaction (see Ref. 3). Also, this feature is found to be a robust property that is present in most applications of tapping-mode AFM. Many studies are based on this behavior of the cantilever (for example, see Refs. 4 and 5). In spite of its importance and prevalence, little insight is present in the literature on this behavior of the cantilever. It is clear that an effective identification framework should explain this feature and exploit it for its purposes.

In this article we provide a feedback perspective of the tapping-mode dynamics. Based on this we develop a set of principles that can be used for identifying the tip–sample interaction. These general tools can be utilized for a wide range of tapping-mode applications. One of the fallouts of the study is the explanation of the near sinusoidal steady-state behavior of the cantilever. We also develop a simple model of the tapping-mode dynamics and apply the developed identification tools to estimate the parameters of the proposed model. It is shown that the identification paradigm developed is powerful and that a simple model can match experimental data remarkably well. The tools also elucidate

[a]Electronic mail: murti@iastate.edu

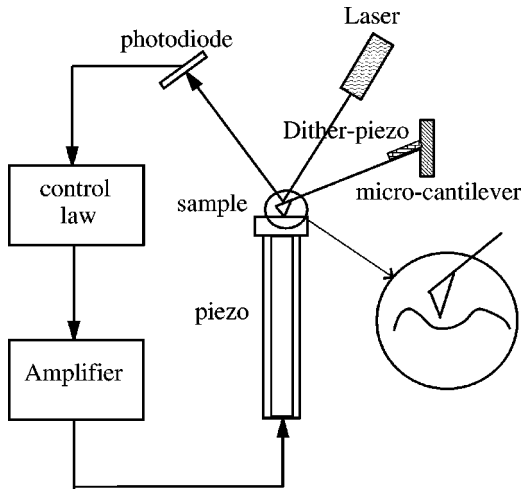

FIG. 1. Experimental setup used. The sample is positioned using a piezo tube. The cantilever is oscillated using a sinusoidal voltage applied to the dither piezo. The displacement of the cantilever is recorded by a laser which reflects off the cantilever surface and is incident into a split photodiode sensor.

the limitations of tapping-mode AFM in identifying the tip–sample potential.

This article is organized as follows. In Sec. II we develop the analytical principles for identification purposes. In Sec. III we present the model of the cantilever and the tip–sample interaction used in this article. We then specialize the identification tools for this model. In Sec. IV we present experimental methods developed and in Sec. V we give results and discussion.

II. ANALYSIS

In the tapping mode, the cantilever in the AFM is forced sinusoidally by a dither piezo attached to the substrate that forms the support of the cantilever (see Fig. 1). The cantilever is thus subjected to the drive force through the dither piezo and the tip–sample interaction force. In addition to these forces the cantilever motion is influenced by the damping force due to the ambient environment and the intrinsic damping caused by the bending of the cantilever beam. We term these dissipative forces collectively as the air damping force.

We assume that a linear time-invariant model G of the cantilever suffices to predict its behavior. Thus G is a linear time-invariant operator which takes the sample and the drive force as its input and provides the tip displacement as its output. Note that G includes the effect of the air damping force. Also note that efficient techniques exist in the literature to obtain a precise model of G (see, for example, Refs. 6 and 7).

The tip–sample interaction force is a function of the tip displacement and possibly of the tip velocity. Let h be the function which maps the tip–sample separation p and its velocity $\dot{p}$ to the force on the cantilever due to the sample. A block diagram depicting the dynamics is given in Fig. 2, where G is any linear time-invariant model of the cantilever and g is the drive force. The nonlinear tip–sample interaction appears as a feedback block. In this perspective the tip–

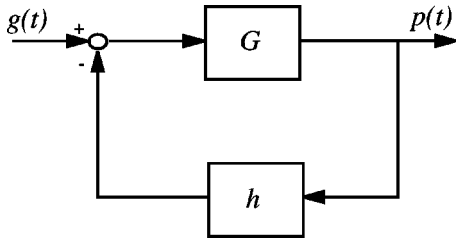

FIG. 2. Block diagram depicting the cantilever dynamics. G is any linear time-invariant model of the cantilever and g is the drive force. The block h models the sample.

sample distance (and possibly velocity) is fed back to the system G (which models the cantilever) through the function h. Note that we are viewing the tapping-mode dynamics as an interconnection of two systems, the system G which models the cantilever and the block h which models the sample.

The harmonic balance equations are derived next (they were first introduced by the authors in Ref. 8). It is shown in Ref. 9 that under unrestrictive assumptions, the tapping-mode dynamics admit a periodic solution with the same period T as that of the sinusoidal forcing g. We denote such a periodic solution by $p_*(t)$. Because the nonlinear force on the cantilever due to the sample is assumed to be time invariant it follows that $h(p_*,\dot{p}_*)$ is also periodic with period T. Thus p_*, $h(p_*,\dot{p}_*)$ and $g(t)$ all admit expansions of the form $p_*(t)=\Sigma_{k=-\infty}^{\infty}p_k e^{jk\omega t}$, $h[p_*(t),\dot{p}_*(t)]=\Sigma_{k=-\infty}^{\infty}h_k e^{jk\omega t}$ and $g(t)=\Sigma_{k=-\infty}^{\infty}g_k e^{jk\omega t}$, where $x_k=x_{kr}+jx_{ki}$ are the exponential Fourier coefficients of x and $\omega=2\pi/T$.

Note that for the periodic solution Fig. 2 can be viewed as illustrated in Fig. 3. Since the cantilever model G is a linear time-invariant system, it follows from the Fourier series properties of linear time-invariant systems that the input and output harmonics of the system are related by

$$G(jk\omega)(-g_k+h_k)+p_k=0, \quad \text{for all } k=0,\pm 1,\pm 2,\ldots. \tag{1}$$

Equation (1) above provides the first principle for tapping-mode dynamics; if the cantilever dynamics (in the sense described above) is linear time invariant and the tip–sample interaction is time invariant then the Fourier coefficients g_k, h_k and p_k of the forcing $g(t)$, tip–sample interaction force on the periodic orbit $h[p_*(t)]$ and the tip displacement $p_*(t)$, respectively, have to obey the harmonic balance equations given by Eq. (1).

In order to verify the harmonic balance equations, data from Ref. 3 were used where advanced models for tip–sample interaction were employed. The tip-sample interaction model given in Ref. 3 captures most of the features seen

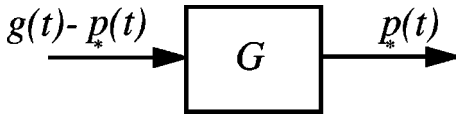

FIG. 3. On the periodic orbit Fig. 2 can be viewed as illustrated above where $g(t)$ is the sinusoidal forcing and $p_*(t)$ is a periodic solution the tapping-mode dynamics admits.

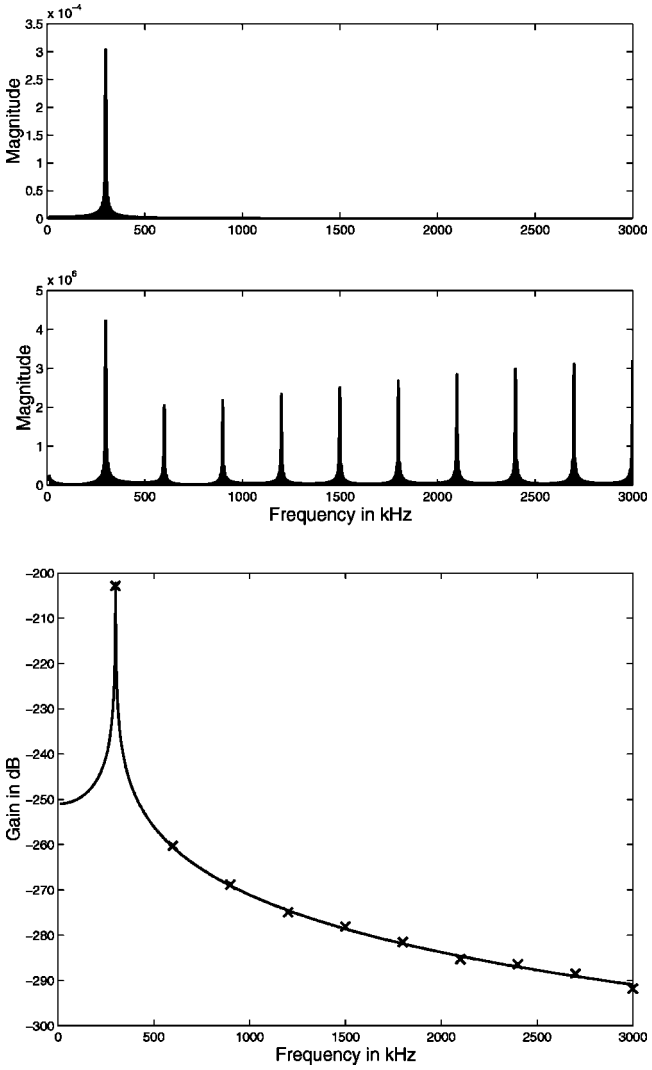

FIG. 4. Magnitude plots of the Fourier transforms of $p(t)$ and $u(t)$ are shown first. The ratios between $|\hat{p}_*(jk\omega)|$ and $|\hat{u}_*(jk\omega)|$ for $k=1,\ldots,10$ are then compared with the corresponding points on the frequency response plot of G thus illustrating the harmonic balance.

in experimental data. The simulation data used correspond to a sinusoidal forcing at a frequency of $\omega=300$ kHz which is the same as the resonant frequency of the cantilever. Let $u(t)=g(t)-h(p_*,\dot{p}_*)$. The magnitudes of the Fourier transforms of the simulation data $p_*(t)$ and $u(t)$ given by $|\hat{p}_*(j\omega)|$ and $|\hat{u}_*(j\omega)|$, respectively, are shown in Fig. 4. Next the ratios between $|\hat{p}_*(jk\omega)|$ and $|\hat{u}_*(jk\omega)|$ for $k=1,\ldots,10$ are compared with the corresponding points on the frequency response plot of G. The remarkable agreement between the two illustrates Eq. (1). The only assumption made for Eq. (1) to be true is that the cantilever dynamics are linear time invariant and that the tip–sample interaction is time invariant. Note that the assumption that the cantilever motion and hence tip–sample interaction are periodic is not a trivial one. We will address this further later in the article. We will now utilize Eq. (1) to develop schemes for identifying the tip–sample interaction.

Note that, in Eq. (1), thermal noise response plots can be used to identify $G(jk\omega)$ (see Refs. 6 and 7). In Eq. (1) the Fourier coefficients of the forcing g_k are known and the Fourier coefficients p_k of the cantilever oscillations can be found by performing a Fourier analysis on the measured cantilever–tip oscillations. Equation (1) can then be used to evaluate h_k. Indeed Eq. (1) can be rewritten as

$$h_k=g_k-\frac{p_k}{G(jk\omega)}, \tag{2}$$

where h_k are the unknowns and the right-hand side of the above equation can be obtained from experimental data. Note that h_k are the Fourier coefficients of $h[p_*(t)]$ where $p_*(t)$ is the steady-state cantilever oscillation. The steady-state periodic orbit of the cantilever depends on the forcing frequency ω, the magnitude of the forcing γ, and the tip–sample offset l. Thus h_k, g_k and p_k are functions of ω,γ and l. By varying each one of these parameters we can evaluate $h_k(\omega,\gamma,l)$ for different values of ω,γ and l. The Fourier coefficients h_k can be processed to provide information about the sample properties that can be used to identify various parameters in a given model of the interaction between the tip and the sample.

Note that any time-invariant model of the tip–sample interaction has to satisfy Eq. (2) if we account for any noise in the detection of $p(t)$. An approach to identifying the tip–sample interaction is to assume a parametric model of the tip–sample interaction which takes in as input the tip displacement and velocity and provides the force on the cantilever due to the sample as its output. Let $H(\Theta)$ denote such a model where Θ is a finite set of parameters. Thus we have $h[p(t)]=H(\Theta)[p(t)]$. The corresponding minimization problem is

$$\min_{\Theta}\sum_{k=0}^{\infty}|H_k-h_k|^2, \tag{3}$$

where H_k are the Fourier coefficients of $H(\Theta)[p(t)]$. Note that the tractability of the problem, Eq. (3) depends on the parametric model H and thus care should be taken so that the resulting minimization problem is solvable. We will follow this approach for identification in Sec. III.

The feedback perspective of Fig. 2 provides significant insights which we present now. In most tapping-mode applications the forcing frequency is close to the resonant frequency of the cantilever. If the forcing frequency is selected to be the resonant frequency, then the thermal noise response plots of a typical cantilever indicate that $|G(jk\omega)|\approx 0$ for $k=2,3,\ldots$ (see Ref. 6). Thus G acts like a low pass filter which ensures that the higher frequency components get filtered. It now follows immediately from Eq. (1) that $p_k\approx 0$ if $|k|\geqslant 2$. Thus one can write

$$p_*(t)=a\cos(\omega t+\phi)+p_0, \tag{4}$$

where $a=2|p_1|$ and $p_1=|p_1|e^{j\phi}$. Thus the filtering effect of the cantilever transfer function results in a nearly sinusoidal orbit of the cantilever. This explains one of the essential features of tapping-mode AFM which is pivotal to its operations. Note that we have assumed that G is a linear time-invariant model of the cantilever. However, for the near sinusoidal behavior of the steady-state oscillations the essential

ingredient is only the low pass property of the cantilever. Note that this also indicates that the higher the quality factor Q the more sinusoidal the resulting steady-state oscillations will be. It is important to remember that this assumes the cantilever motion to be periodic (precluding, for example, cases where the cantilever hits the sample only every third cycle). Such cases can occur. For example, the side bands around the peak in Fig. 1(d) of Ref. 5 indicate nonperiodic motion. However the power carried in the side bands is small compared to that in the central peak. The power carried in the higher harmonics is quite small as well. Thus the harmonic balance should work well on the first harmonic.

A limitation of the tapping-mode AFM in identifying the tip–sample interaction is also indicated by the above discussion. Note that the cantilever tip oscillation (which is the measured signal) contains negligible information on the high frequency content of $h[p_*(t)]$, because such information is filtered out by the cantilever. Thus the tapping-mode AFM can be utilized to identify the tip–sample interaction only up to the first harmonic of $h[p_*(t)]$.

Now we introduce a power balance technique for tapping-mode AFM.[5] This technique is based on the fact that at steady state the average rate at which energy is fed into the cantilever must equal the average rate at which energy is dissipated by the cantilever. The instantaneous power delivered by the driver is the force on the driver (f_{drive}) times the velocity of the driver as given by

$$P_{\text{in}}=\frac{1}{m}f_{\text{drive}}\dot{b}(t). \tag{5}$$

Similarly P_d and P_t are given by

$$P_d=\frac{1}{m}f_{\text{damp}}\dot{p}_*(t), \tag{6}$$

$$P_t=\frac{1}{m}f_{\text{int}}\dot{p}_*(t), \tag{7}$$

where f_{damp} is the damping force and f_{int} is the tip–sample interaction force, respectively. $\overline{P_{\text{in}}}$, $\overline{P_d}$ and $\overline{P_t}$ are obtained by averaging P_{in}, P_d and P_t over one cycle of the cantilever oscillation, respectively. The fact that energy is conserved results in

$$\overline{P_{\text{in}}}=\overline{P_d}+\overline{P_t}. \tag{8}$$

From knowledge of the tip motion $p_*(t)$ and the cantilever model $G(j\omega)$ we can evaluate $\overline{P_{\text{in}}}$ and $\overline{P_d}$. Using Eq. (8) we can evaluate $\overline{P_t}$. As will be seen later, this forms another tool with which to identify the parameters of the tip–sample interaction.

III. CANTILEVER AND TIP–SAMPLE INTERACTION MODEL

We now apply the harmonic and power balance tools to the tapping-mode dynamics assuming a model for the cantilever and a model for the tip–sample interaction. For most applications the dynamical equation for the displacement of the cantilever is well modeled by

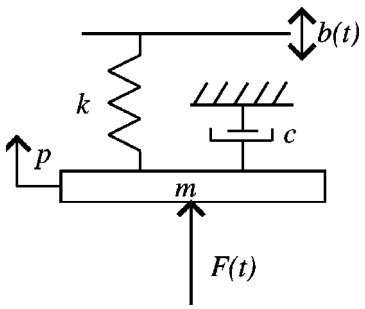

FIG. 5. Model of the cantilever. F is the force on the cantilever due to the sample and b describes the displacement of the base of the cantilever.

$$\ddot{p}+2\xi\omega_0\dot{p}+\omega_0^2 p+h(p,\dot{p})=g(t), \tag{9}$$

where $\omega_0=\sqrt{k/m}$, $2\xi\omega_0=c/m$ and $g(t)=kb(t)/m$ and h is the force due to the sample per unit mass that is assumed to be dependent only on the position and velocity of the cantilever tip. The cantilever model dynamics are described by Fig. 5. Assuming the second-order model described by Eq. (9) and that the sinusoidal nature of the tip displacement given by Eq. (4) are true, the harmonic balance equations (1) reduce to

$$h_0-g_0+\omega_0^2 p_0=0, \tag{10}$$

$$h_{1r}(a,\phi,p_0)-g_{1r}+\Omega\frac{a}{2}\cos\phi-2\xi\omega\omega_0\frac{a}{2}\sin\phi=0, \tag{11}$$

$$h_{1i}(a,\phi,p_0)-g_{1i}+2\xi\omega\omega_0\frac{a}{2}\cos\phi+\Omega\frac{a}{2}\sin\phi=0, \tag{12}$$

where $\Omega=\omega_0^2-\omega^2$. Note that $p_{1r}=(a/2)\cos\phi$ and $p_{1i}=(a/2)\sin\phi$. Also, for the second-order model of the cantilever given by Eq. (9), $G(j\omega)=1/(-\omega^2+j2\xi\omega\omega_0+\omega_0^2)$.

Let the dither forcing function be given by $b(t)=a_d\cos(\omega t)$ (note that $a_d=\gamma/\omega_0^2$) and the steady-state sinusoidal orbit be given by $p_*(t)=a\cos(\omega t+\phi)+p_0$ where a is the amplitude of the cantilever, ϕ is the phase difference between $p_*(t)$ and $b(t)$ and p_0 is the dc offset. Averaging Eq. (5) over a complete cycle we obtain $\overline{P_{\text{in}}}$ to be

$$\overline{P_{\text{in}}}=-\frac{1}{2}\frac{k}{m}a_d a\omega\sin(\phi). \tag{13}$$

Similarly $\overline{P_{\text{air}}}$ is given by

$$\overline{P_{\text{air}}}=\frac{1}{2}\frac{c}{m}a^2\omega^2. \tag{14}$$

From Eq. (8)

$$\overline{P_{\text{tip}}}=-\frac{1}{2m}\frac{ka^2\omega}{Q}\left(\frac{Qa_d\sin(\phi)}{a}+\frac{\omega}{\omega_0}\right). \tag{15}$$

If the drive frequency is chosen to be ω_0, Eq. (15) reduces to

$$\overline{P_{\text{tip}}}=-\frac{1}{2m}\frac{ka^2\omega_0}{Q}\left(\frac{a_0}{a}\sin(\phi)+1\right), \tag{16}$$

where $a_0=Qa_d$ is the resonance amplitude of the cantilever when not subjected to the sample influence with $\omega=\omega_0$ and

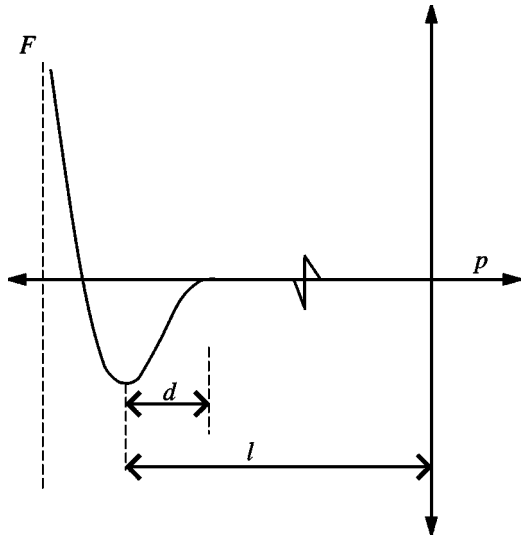

FIG. 6. Sketch of typical cantilever–sample force as a function of position. It indicates long range attractive forces and short range strong repulsive forces.

$$Q=\frac{k}{c\omega_0}=\frac{1}{2\xi}=\frac{\sqrt{km}}{c}. \tag{17}$$

For a conservative system, $\overline{P_{\text{tip}}}$ is equal to zero since there is no dissipation in the sample. Thus Eq. (16) shows that the plot of $-\sin\phi$ against a/a_0 will have a slope of 1 for a conservative system (see Ref. 5 for more details). Hence a deviation from a slope of 1 is likely to indicate power dissipation in the sample. In most experiments the $-\sin\phi$ V s a/a_0 plot is still linear and has a slope considerably less than 1 indicating significant energy dissipation.

A model for the nonlinear tip–sample interaction force (denoted by h) is developed next. Experimental data have indicated that a force curve of the form shown in Fig. 6 characterizes the force on the cantilever due to the sample well. It indicates long range attractive forces and short range strong repulsive forces. We assume a piecewise linear cantilever tip–sample force curve. The additional assumption that the interaction force is also a function of the velocity of the cantilever tip is made.

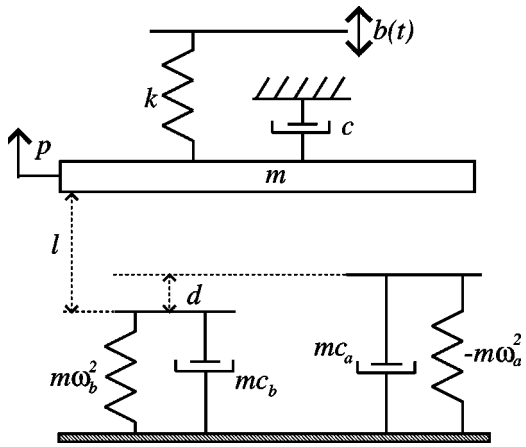

FIG. 7. Model with the piecewise linear cantilever–sample force interaction. When the mass is displaced in the negative direction, first it will encounter the attractive forces modeled by a damper and a negative spring. If the displacement of the mass exceeds l it will encounter repulsive forces modeled by a damper and a positive spring. The dampers account for the energy dissipation due to sample interaction.

The model of the tapping-mode dynamics with the piecewise linear interaction is described in Fig. 7. The negative spring accounts for long range attractive forces and the positive spring accounts for the short range strong repulsive forces. The dampers will account for the energy dissipation in the sample. The variable l will characterize the tip–sample separation. Specifically, we assume that

$$h(p,\dot{p})=0, \quad \text{if } p\geqslant -l+d \tag{18}$$

$$=-\omega_a^2(p+l-d)+c_a\dot{p}, \quad \text{if } -l\leqslant p<-(l-d) \tag{19}$$

$$=\omega_b^2(p+l)-\omega_a^2(p+l-d)+c_a\dot{p}+c_b\dot{p}, \quad \text{if } p<-l. \tag{20}$$

When p is periodic, h is periodic and the Fourier coefficients h_0 and h_1 of the periodic function $h(p,\dot{p})$ when $p(t)=a\cos(\omega t+\phi)+p_0$ are given by

$$\begin{aligned} h_0(a,p_0)&=0, \quad \text{if } p_0-a\geqslant -l+d\\ &=\frac{a\omega_a^2}{\pi}\left(\sqrt{1-s_1^2}-|s_1|\cos^{-1}(|s_1|)\right),\\ &\quad \text{if } -l\leqslant p_0-a\leqslant l+d\\ &=\frac{a\omega_a^2}{\pi}\left(\sqrt{1-s_1^2}-|s_1|\cos^{-1}(|s_1|)\right)-\frac{a\omega_b^2}{\pi}\\ &\quad\times\left(\sqrt{1-s_2^2}-|s_2|\cos^{-1}(|s_2|)\right), \quad \text{if } p_0-a\leqslant l. \end{aligned} \tag{21}$$

$$\begin{aligned} h_{1r}(a,p_0,\phi)&=0, \quad \text{if } p_0-a\geqslant -l+d\\ &=\frac{a\cos\phi}{2}\frac{\omega_a^2}{\pi}c_1+\frac{a\sin\phi}{2}\frac{\omega c_a}{\pi}c_1,\\ &\quad \text{if } -l\leqslant p_0-a\leqslant l+d\\ &=\frac{a\cos\phi}{2}\frac{\omega_a^2}{\pi}c_1-\frac{a\cos\phi}{2}\frac{\omega_b^2}{\pi}c_2\\ &\quad+\frac{a\sin\phi}{2}\frac{\omega c_a}{\pi}c_1+\frac{a\sin\phi}{2}\frac{\omega c_b}{\pi}c_2,\\ &\quad \text{if } p_0-a\leqslant l. \end{aligned} \tag{22}$$

$$\begin{aligned} h_{1i}(a,p_0,\phi)&=0, \quad \text{if } p_0-a\geqslant -l+d\\ &=\frac{a\sin\phi}{2}\frac{\omega_a^2}{\pi}c_1-\frac{a\cos\phi}{2}\frac{\omega c_a}{\pi}c_1,\\ &\quad \text{if } -l\leqslant p_0-a\leqslant -l+d\\ &=\frac{a\sin\phi}{2}\frac{\omega_a^2}{\pi}c_1-\frac{a\sin\phi}{2}\frac{\omega_b^2}{\pi}c_2\\ &\quad-\frac{a\cos\phi}{2}\frac{\omega c_a}{\pi}c_1-\frac{a\cos\phi}{2}\frac{\omega c_b}{\pi}c_2,\\ &\quad \text{if } p_0-a\leqslant -l \end{aligned} \tag{23}$$

with $c_1=|s_1|\sqrt{(1-s_1^2)}-\cos^{-1}(|s_1|)$, $c_2=|s_2|\sqrt{(1-s_2^2)}-\cos^{-1}(|s_2|)$, $s_1=(-l+d-p_0)/a$, and $s_2=(-l-p_0)/a$.

Note that in the above identities ω_a^2, ω_b^2, c_a and c_b are the parameters of the model which appear linearly. This results in a tractable optimization problem, Eq. (3). Also, using the piecewise linear model for the nonlinear interaction, closed-form expressions were obtained for the various power components involved in the power balance equation given by Eq. (8). Note that we can split $\overline{P_{\text{tip}}}$ into the average power dissipated due to the damper mc_a, $\overline{P_{\text{att}}}$ and the power dissipated due to the damper mc_b, P_{rep}, P_{att} and P_{rep} are evaluated to be

$$\overline{P_{\text{att}}}=\frac{1}{2}c_a a^2\omega^2\left(\frac{\cos^{-1}(|s_1|-|s_1|\sqrt{(1-s_1^2)})}{\pi}\right),$$
$$\overline{P_{\text{rep}}}=\frac{1}{2}c_b a^2\omega^2\left(\frac{\cos^{-1}(|s_2|-|s_2|\sqrt{(1-s_2^2)})}{\pi}\right). \tag{24}$$

The power balance equation can be rewritten as

$$\overline{P_{\text{in}}-P_{\text{air}}=P_{\text{att}}+P_{\text{rep}}}. \tag{25}$$

If the amplitude, phase and p_0 are measured experimentally, the zeroth- and the first-order Fourier coefficients h_0 and h_1 of the tip–sample interaction force h can be evaluated by solving the harmonic balance equations [Eqs. (10)–(12)]. This process can be repeated at various tip–sample separations. The values of h_0 and h_1 thus obtained together with Eqs. (21)–(23) provide a tool for the estimation of the tip–sample interaction model parameters. Also, $\overline{P_{\text{in}}}$ and $\overline{P_{\text{air}}}$ can be evaluated using Eqs. (13) and (14). Hence Eqs. (24) and (25) will form another set of tools for the analysis of experimental data.

IV. EXPERIMENTAL METHODS

Experiments were performed on silicon, mica, high density polyethylene and low density polyethylene. A Multi-Mode scanning probe microscope from Digital Instruments was used for the experiments. Here one of the experiments performed on silicon is presented. (The results of this experiment were first reported in Ref. 5.)

An atomic force microscope (Multi-Mode, Digital Instruments, Santa Barbara, CA) was operated in the tapping mode. A silicon cantilever 225 μm in length was used. The model parameters were evaluated by analyzing the cantilever response to thermal noise (see Refs. 6 and 7). The parameters were identified to be $\xi=0.0038$, $\omega_0=2\pi\times 73881$ rad/s, and $k=4$ N/m. A sinusoidal voltage with its frequency equal to ω_0 was applied to the dither piezo. The sample (a silicon wafer) initially was sufficiently far from the cantilever so that it did not affect the cantilever motion. Once the cantilever reached its steady state, the sample was slowly moved towards the vibrating cantilever by extending the piezo. The motion of the cantilever tip at various values of the piezo extension was recorded using the HP 89410 vector signal analyzer.

V. RESULTS AND DISCUSSION

For the piecewise tip–sample interaction model there are five parameters to be estimated, namely, the length of the attractive region d (the attractive region is where the phase difference is less than $-90°$), the attractive and repulsive spring constants per unit mass, ω_a^2 and ω_b^2 and the damper values per unit mass, c_a and c_b. The estimation is based on data obtained by varying l and by fixing the magnitude of forcing a_d and the frequency of the forcing at the first resonant frequency of the cantilever.

The first parameter estimated is the length of the attractive region, d. Note that the absolute tip–sample separation is not available experimentally. What can be measured is the photodiode output in volts (denoted by V_a) which is a measure of the vibration amplitude, a and the differential motion, Δl of the piezo actuator which positions the sample. The assumption that the amplitude equals the tip–sample separation in the repulsive region is made. This is justified because the penetration of the tip into this region is small due to the very strong repulsive forces in most samples. From this assumption, $\Delta a/\Delta l$ equals 1 in the repulsive region where Δa is the change in amplitude and Δl is the change in the separation. Hence,

$$\frac{dV_a}{dl}\frac{da}{dV_a}=\frac{da}{dl}=1. \tag{26}$$

Since dV_a/dl, which is the slope of the photodiode output versus the separation curve, can be obtained experimentally, da/dV_a which is the sensitivity denoted by S can be calculated from Eq. (26). Using S and the experimentally obtained value V_a, the amplitude a is obtained in nanometers. Again by the assumption that the tip extension into the repulsive region is negligible, the absolute tip–sample separation l is obtained from the relative separation by making the tip–sample separation and amplitude values coincide in the repulsive region. The next step is to identify the minimum separation possible to keep the cantilever freely oscillating. Let this separation be l_0. The freely vibrating amplitude a_0 when subtracted from l_0 gives d. The estimated value from the experimental data is 1.695 nm.

The data points from the attractive region are used to estimate c_a using the power balance equation, Eq. (8). Equation (8) is first used to obtain the value of $\overline{P_{\text{tip}}}$ which is equal to $\overline{P_{\text{att}}}$. The assumption that p_0 values are negligible compared to the amount by which the tip penetrates into the attractive region is made and is justified by the simulation data of Ref. 3. Note that due to the small magnitude of p_0 in typical tapping-mode applications, it is difficult to measure p_0. The linear relationship between the $\overline{P_{\text{att}}}$ and the c_a evident from Eq. (24) is exploited to obtain a least square estimate of c_a. A value of $3e-7$ μs^{-1} was obtained which is approximated by 0 μs^{-1}. Even though for this experimental data a c_a value of approximately zero was obtained, in other experiments on softer samples, higher values for the attractive region damper were obtained.

Once the parameter c_a has been estimated the harmonic balance equations can be used to estimate ω_a. There is a linear relationship between the real and imaginary parts of

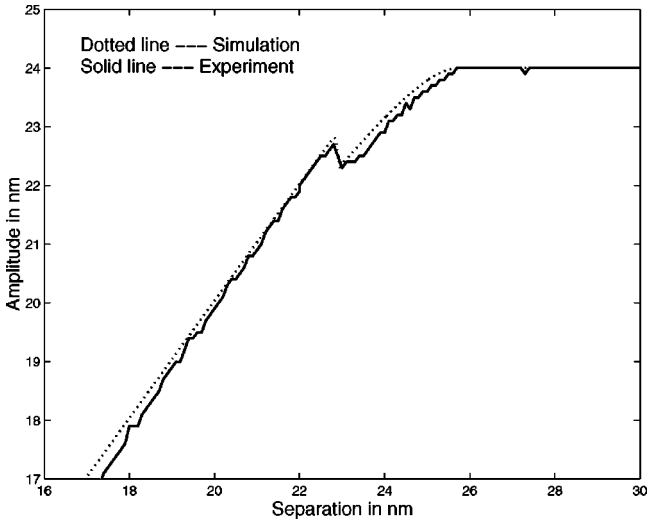

FIG. 8. Using the estimated parameter values simulations are performed and the plots thus obtained are compared with those obtained through experiments. Here the amplitude is plotted against the separation. There is remarkable agreement between the two plots.

the Fourier coefficients of $h(p,\dot{p})$ and ω_a^2, Eqs. (22) and (23). For the estimation of this parameter data points were chosen from the attractive region. p_0 is assumed to be zero. The harmonic balance equations given by Eqs. (11) and (12) were used to evaluate h_{1r} and h_{1i} directly from the amplitude and phase data. h_0 was not used for estimation since it is very sensitive to p_0 values. The problem is set up in the framework of least square estimation [see Eq. (3) and Ref. 10]. The value of ω_a was estimated to be 0.31 μs^{-1}.

The estimation of attractive region related parameters is fairly robust since the effect of p_0 on them is negligible. However the strong dependence of c_b and ω_b on p_0 values makes the estimation of repulsive region parameters difficult. This dependence is due to the fact that the amount of penetration of the tip into the repulsive region is of the order of p_0 unlike in the attractive region.

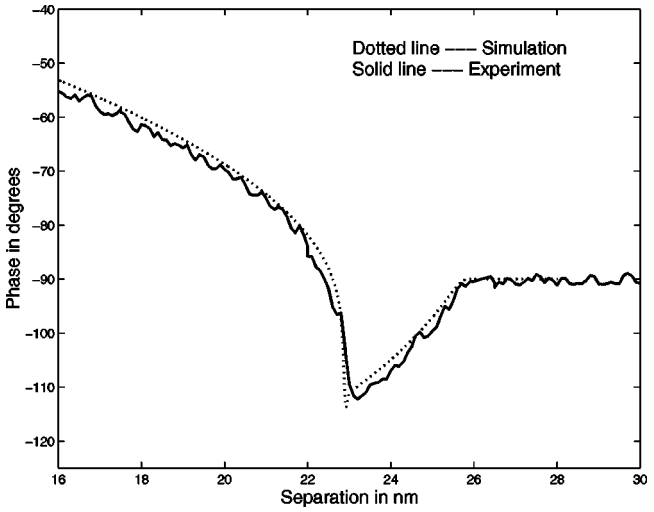

FIG. 9. Phase plotted against the separation l. Here also the two plots show a good match.

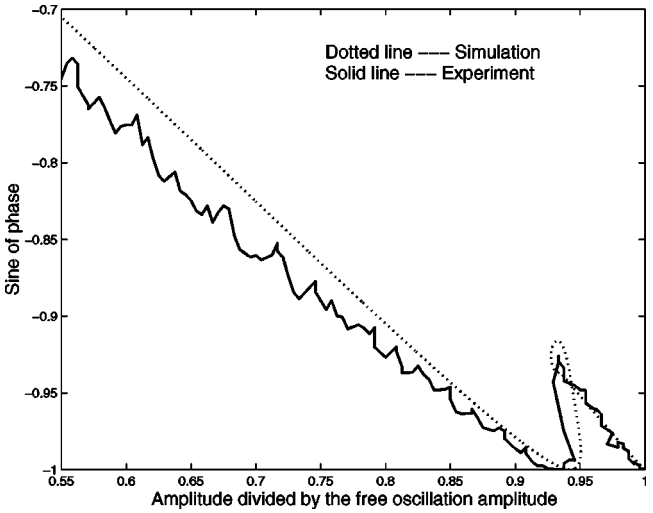

FIG. 10. $\sin\phi$ plotted against a/a_0. It can be seen that the model captures the linearity of this plot and even the reduction in the slope from 1.

A reasonable estimate for c_b can be obtained by observing the slope of the $\sin\phi$ vs a/a_0 plot in the repulsive region. The c_b value of 1.45 μs^{-1} was fixed by comparing the slope of the simulation plots with that of the experimental plot.

Once c_b is fixed, the p_0 dependent term in the expression for P_{rep} can be estimated for each amplitude and phase value using the power balance equations [Eqs. (8) and (24)]. Now a similar procedure as that for the estimation of ω_a can be employed, the difference being that the estimation is done using data from the repulsive region. ω_b was obtained to be 2.7 μs^{-1}. Simulations show that a higher ω_b value is desirable. A value of 3.03 μs^{-1} was found to be a good choice.

As mentioned earlier, the strong dependence of c_b and ω_b on p_0 makes their estimation more difficult. Therefore trial and error iterations on the estimated values may be required for the repulsive region parameters. Also the assumption made that the amplitude equals l in the repulsive region may have an effect on the estimation of the repulsive region parameters. Hence the procedure outlined here is more suitable for the estimation of the attractive region parameters.

The estimated parameters were used to simulate the AFM operating in tapping mode. The corresponding results were compared with those obtained experimentally. The values of the various parameters used for simulations are $\omega_a = 0.31$ (attractive spring constant of 1.78 N/m), $\omega_b = 3.03$ (repulsive spring constant of 170.42 N/m), and $c_a = 0$ μs^{-1} and $c_b = 1.45$ μs^{-1}. The corresponding plots are shown in Figs. 8–10. It is evident from the plots that the model agrees with the experimental data. The most remarkable feature is that a simple model can capture the behavior of the tapping-mode AFM. The fact that a piecewise linear model for tip–sample interaction suffices to predict the essential features of the tapping-mode AFM also indicates the limitation of using tapping-mode AFM to identify tip–sample interaction. As mentioned before the high frequency content of the tip–sample interaction force is filtered out by the cantilever thus making it unsuitable for identifying the finer features of the tip–sample potential curve.

In conclusion the feedback perspective together with the

harmonic and power balance tools provide an effective method by which to identify the tip–sample interaction. The feedback perspective with the cantilever viewed as a filter explains the sinusoidal nature of the steady-state oscillations of the cantilever tip. The harmonic and power balance principles are applicable to a diverse range of tapping-mode operating conditions. Note that in identifying the model used in this article it was assumed that the tip oscillations are sinusoidal. Only the first harmonic data were utilized in identifying the model parameters. However, if it is possible to measure the higher harmonics of the cantilever oscillations then this data can be easily incorporated into the modeling process by utilizing Eqs. (1) and (8). Note also that the harmonic and power balance methods are general tools which can be applied to a different model than the one provided here. The directions indicated above will be pursued in future research.

ACKNOWLEDGMENTS

This research was supported by National Science Foundation (NSF) Grant No. ECS-9733802 to one of the authors (M.V.S). The authors thank Dr. Ken Babcock and Dr. Sergei N. Magonov of Digital Instruments for all the assistance during the research. They would also like to thank Dr. Boris Anczykowski for providing them with the data from Ref. 3.

[1] G. Binnig, C. Quate, and C. Gerber, Phys. Rev. Lett. **56**, 930 (1986).
[2] Q. Zhong, D. Inniss, K. Kjoller, and V. Elings, Surf. Sci. **290**, L688 (1993).
[3] B. Anczykowski, D. Kruger, K. L. Babcock, and H. Fuchs, Ultramicroscopy **66**, 251 (1996).
[4] U. Durig, Appl. Phys. Lett. **76**, 1203 (2000).
[5] J. P. Cleveland, B. Anczykowski, A. E. Schmid, and V. B. Elings, Appl. Phys. Lett. **72**, 2613 (1998).
[6] M. V. Salapaka, H. S. Bergh, J. Lai, A. Majumdar, and E. McFarland, J. Appl. Phys. **81**, 2480 (1997).
[7] D. A. Walters, J. P. Cleveland, N. H. Thomson, P. K. Hansma, M. A. Wendman, G. Gurley, and V. Elings, Rev. Sci. Instrum. **67**, 3583 (1996).
[8] A. Sebastian, M. V. Salapaka, D. J. Chen, and J. P. Cleveland, Proceedings of the American Control Conference, San Diego, CA, 1999.
[9] M. V. Salapaka, D. Chen, and J. P. Cleveland, Phys. Rev. B **61**, 1106 (2000).
[10] D. G. Luenberger, *Optimization by Vector Space Methods* (Wiley, New York, 1969).